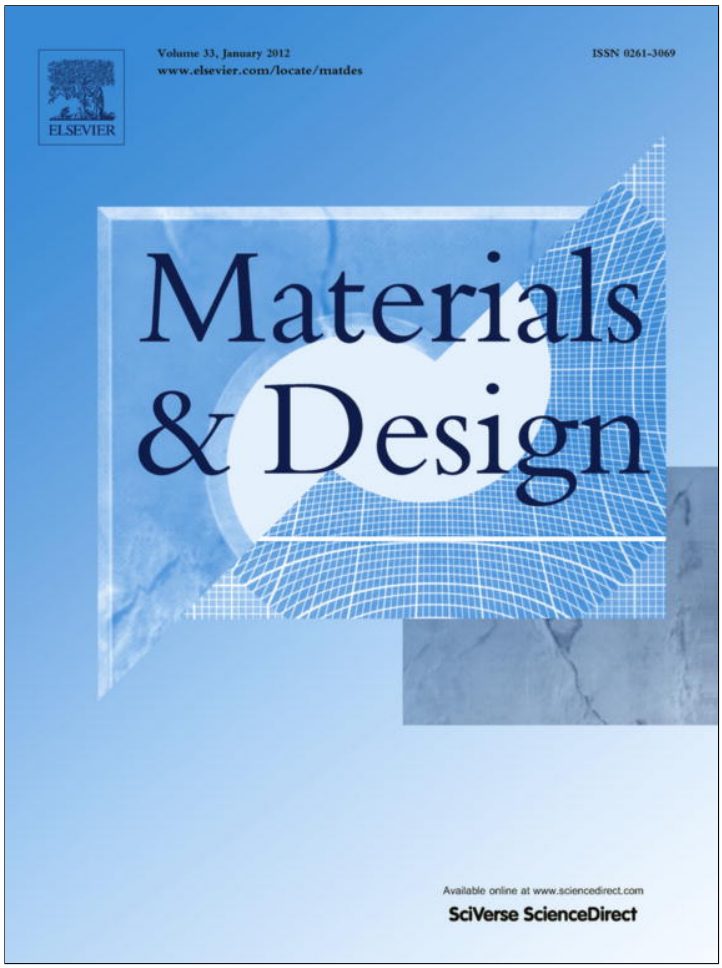

(This is a sample cover image for this issue. The actual cover is not yet available at this time.)

Materials and Design 44 (2013) 397–406

Contents lists available at SciVerse ScienceDirect

Materials and Design

journal homepage: www.elsevier.com/locate/matdes

Real microstructure based micromechanical model to simulate microstructural level deformation behavior and failure initiation in DP 590 steel

Surajit Kumar Paul *

R&D, Tata Steel Limited, Jamshedpur 831 001, India

ARTICLE INFO

Article history:
Received 19 June 2012
Accepted 10 August 2012
Available online 21 August 2012

Keywords:
Dual phase steel
Strain partitioning
Strain localization
Damage
Volume expansion of martensite
Failure modes

ABSTRACT

Dual phase (DP) steels having a microstructure consists of a ferrite matrix, in which particles of martensite are dispersed, have received a great deal of attention due to their useful combination of high strength, high work hardening rate and ductility. In the present work, a microstructure based micromechanical model is developed to capture the deformation behavior, plastic strain localization and plastic instability of DP 590 steel. A microstructure based approach by means of representative volume element (RVE) is employed for this purpose. Dislocation based model is implemented to predict the flow behavior of the single phases. Plastic strain localization which arises due to incompatible deformation between the hard martensite and soft ferrite phases is predicted for DP 590 steel. Different failure modes arise from plastic strain localization in DP 590 steel are investigated on the actual microstructure by finite element method.

1. Introduction

Over the last decade, a strong competition between steel and low density metal industries has been observed as a result of increasing requirements of passenger safety, vehicle performance and fuel economy. The response of steel industry to the new challenges is a rapid development of higher strength steels, named advanced high strength steels (AHSSs). These steels are characterized by improved formability and crashworthiness compared to conventional type steel grades. The category of AHSS covers the following generic types: dual phase (DP), transformation induced plasticity (TRIP), complex phase (CP) and martensitic steels (MART). Among AHSS, dual phase (DP) steels are mostly used in automotive industries due to its low yield strength, high work hardening rate and superior formability [1,2]. In general, DP steels are produced by the intercritical heat treatment of low carbon steel, and they consist of composite microstructure of soft ferrite matrix and hard martensite. The flow behavior of dual-phase steels not only depends on the properties of ferrite and martensite but also on the volume fraction and morphology of the martensite islands [3–5], and the partitioning of stress and strain between the two phases during deformation [6–9].

Tremendous efforts have been made by many researchers on exploring various aspects of DP steels. The effect of volume fraction (V_m) of the harder phase (martensite) has been investigated by different authors [4,10,11]. Increasing the volume fraction of the harder phase was found to increase the yield strength and ultimate tensile strength of the aggregate. Bag et al. [4] reported that the increase in strength with V_m only extends up to $V_m \approx 55\%$, after which a reduction in strength is observed. Shen et al. [12] have shown, using a scanning electron microscope equipped with a tensile straining stage, that the distribution of the strains between the ferrite and martensite phases, as well as among the different grains of each phase was observed to be inhomogeneous. They observed that the ferrite phase deformed immediately and with a much more rapid rate than the delayed deformation of the martensite. They had also shown, using scanning electron microscopy that at low V_m only the ferrite matrix deforms, with no measurable strain occurring in the martensite particles. At high V_m, however, they had shown that shearing of the interface between the martensite and ferrite occurs extending the strain into the martensite islands after the ferrite matrix is excessively strained, which is in agreement with Rashid and Cprek [13]. The different stages of strain hardening have been attributed [4,11,13] to the following phases of deformation: (a) both component phases are elastic, (b) the softer phase deforms plastically while the harder phase deforms only elastically and (c) both components deform plastically. Because the flow strength of ferrite is much lower than that of martensite, plastic deformation begins in the soft ferrite. This plastic deformation in the ferrite phase is constrained by the adjacent martensite, leading to localize the deformation in the ferrite. Thus the localized deformation in the ferrite leads to fracture of the DP steel which occurs by decohesion of ferrite–martensite interface or void nucleation and coalescence depending of the morphological difference.

* Address: Research and Development, Tata steel Limited, Jamshedpur 831 001, India. Tel.: +91 657 2148919/13, mobile: +91 9939632284; fax: +91 657 2271748.
E-mail addresses: paulsurajit@yahoo.co.in, surajit.paul@tatasteel.com

0261-3069/$ - see front matter © 2012 Elsevier Ltd. All rights reserved.
http://dx.doi.org/10.1016/j.matdes.2012.08.023

The strength of martensite depends primarily on its carbon content [5,14]. Whereas, in general the strength of ferrite depends on its composition, and grain size [4,9]. It is now established that the martensite volume fraction is dominant in controlling the tensile properties and increasing the amount of martensite decreases ductility. The previous studies were shown that the morphology of martensite particles also plays an important role in the strength and ductility of the dual phase steels [2,3]. For a constant volume fraction of martensite, a microstructure of finely dispersed martensite has a better combination of strength and ductility. In DP steel the ferrite gets additional strength from the initial dislocation density i.e. strain field, created due to the compatibility stresses and strains when austenite transforms into martensite during cooling [15,16]. This additional strengthening of ferrite adjacent to martensite also causes gradual yielding of DP steels.

Ductile damage/failure can be caused by main three reasons, they are: initial geometrical imperfections [17], void initiation growth and coalescence [18–20] and deformation localization due to microstructure-level inhomogeneity [21–25]. Sun et al. [22,23] have developed a microstructure-based modeling procedure in which the failure mode and ultimate ductility of DP steels are predicted under different loading conditions using the deformation/plastic strain localization theory. Ductile failure is predicted as the natural outcome of the plastic strain localization due to the incompatible deformation between the hard martensite phase and the soft ferrite phase. Similar microstructure-based finite element analysis was used by Choi et al. [24] in predicting the ductility and failure modes of transformation induced plasticity (TRIP) steel. Sun et al. [22] also reported that when the volume fraction of martensite is above 15%, the pre-existing voids in the ferrite matrix does not significantly reduce the overall ductility of the DP steels, and the overall ductility is more influenced by the mechanical property disparity between the two phases.

Strain localization is the earliest stage of fracture process. Strain localization normally leads to localized increase of stress–strain in a particular zone and decrease (i.e. unloading) of stress–strain in the remaining zone. If once strain localization is initiated then, final fracture (i.e. initiation and separation of surfaces) occurs quickly in that localized zone by initiation, growth and coalition of voids or decohesion of ferrite–martensite interface. By knowing the importance of strain localization in fracture process many researchers studied strain localization on different steels; they are DP steels [22,23,26,27], TWIP steels [24], Ferrite–pearlite steel [28], etc. In this work, flow behavior and plastic strain localization of DP 590 steel is investigated.

2. Materials used

DP 590 steel which obtained from USA source in the form of cold rolled strips of 1.00 mm thickness, is used for this investigation. The chemical compositions of DP 590 steel is listed in Table 1.

Tensile specimens of 50 mm gauge length and 12.5 mm gauge width (ASTM E8 [29]) were machined parallel to the rolling direction from the as-received steel sheets. All samples were tested at room temperature using an electro-mechanical tensile testing machine at a crosshead speed of 1 mm min^{-1} which roughly corresponds to a strain rate of 3.33×10^{-4} s^{-1}. For scanning electron microscopy (SEM), the usual 2% nital etched specimens were used. SEM microstructure of DP 590 steel is shown in Fig. 1.

Table 1
Composition of DP 590 steel used, in weight percent.

Steel	C	Si	Mn	Al	P	S	Cu	Cr	N
DP 590	0.09	0.35	0.89	0.04	0.015	0.008	0.025	0.022	0.0054

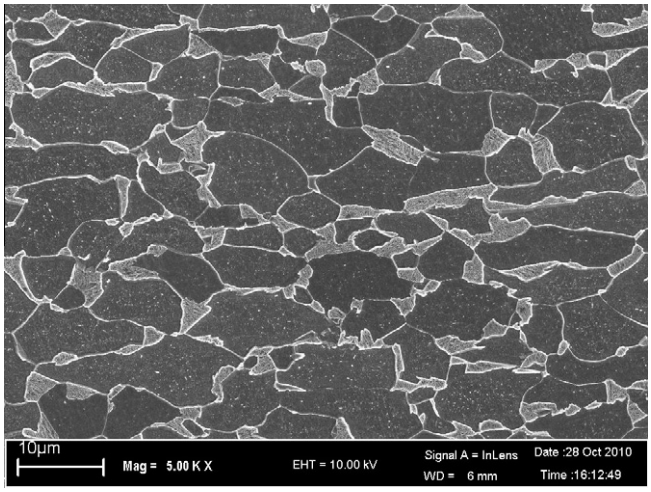

Fig. 1. SEM microstructure of DP 590 steel.

3. Result and discussion

3.1. Constitutive description

In the micromechanical model, the constitutive behavior of the constituent phases will only be required to investigate the aggregate behavior. The interaction of phases (interface boundaries) will be ignored, as it is considerably small, on the order of few atomic sizes, compared to the phases being modeled.

In the elastic–plastic finite element model, von Mises yield criteria, associative flow rule and isotropic hardening rule are assumed for each single phase. To define the isotropic hardening behavior of each individual phase in the calculations, a model based on dislocation theory [27,30,31] is used. The stress–strain relation can be written as

$$\sigma = \sigma_y + \alpha M G \sqrt{b} \sqrt{\frac{1 - \exp(-M K_r \varepsilon)}{K_r L}} \tag{1}$$

where σ is the flow stress at true strain of ε. The explanations of each term are given below and the used values are obtained from a previous study [31]. The second term in Eq. (1) takes care of the dislocation strengthening as well as work softening due to recovery. where α is a constant having a value of 0.33, M is the Taylor factor ($M = 3$), G is the shear modulus ($G = 80$ GPa), b is the Burger's vector ($b = 2.5 \times 10^{-10}$ m), k_r is the recovery rate (for feritte, $k_r = 10^{-5}/d_\alpha$, and for martensite $k_r = 41$). where d_α (m) is the ferrite grain size. L is the dislocation mean free path. For martensite $L = 3.8 \times 10^{-8}$ m [31].

The first term in Eq. (1) is the yield stress which is the summation of friction stress, solid solution strengthening, precipitation strengthening with Nb, Ti and/or V, grain size [32], and it can be described as

$$\sigma_y = 70 + 37\mathrm{Mn} + 83\mathrm{Si} + 2918\mathrm{N}_{sol} + 33\mathrm{Ni} - 30\mathrm{Cr} + 680\mathrm{P} + 38\mathrm{Cu} + 11\mathrm{Mo} + 5000\mathrm{C} + \frac{15.1}{\sqrt{d}} \tag{2}$$

where the first term (70 MPa) is the stress friction value, d (mm) is the grain Size (mm), alloy content (wt%).

This ferrite–martensite microstructure is obtained by intercritical annealing in the austenite–ferrite region followed by

accelerated cooling or water quenching. The resultant austenite to martensite transformation is accompanied by a 2–4% volume increase. The volume expansion during austenite to martensite transformation depends upon the carbon content and can be expressed as [33]

$$\Delta V = 4.64 - 0.53C \quad (3)$$

where ΔV is the specific volume change after quenching due to austenite to martensite transformation, and C is the carbon content (wt%).

3.2. Microscopic simulation with a 3D RVE

Here, a three dimensional RVE (similar to Uthaisangsuk et al. [31]) is used to describe the microstructure on a micro-level. Results from the metallography analysis exhibited the averaged martensitic phase percentage is 10% in DP 590 steel. In the RVE, 10% martensitic phase is randomly distributed in 90% ferrite matrix, which is depicted in Fig. 2. Finite element simulation has been conducted in ABAQUS [34]. Flow behaviors of ferrite and martensite phases in DP 590 steel are determined from Eq. (1) and plotted in Fig. 3. Simulated flow curve determined from 3D RVE matched well with experimental curve Fig. 4. No separate damage law is introduced during 3D RVE simulation. The 3D RVE shows necking which is solely due to strain partitioning among hard martensite and soft ferrite, and followed by strain localization in ferrite arises from strain partitioning. The 3D RVE simulation shows slightly delay in necking. Damage evolution in DP steel arises apart from strain localization are cracking of martensite island, decohesion of martensite interface with matrix, etc. Delay in necking during 3D RVE simulation can be explained as other damaging mechanisms in DP steel are not considered in simulation.

3D RVE simulations are done in two ways, with and without considering martensite volume expansion. 3D RVE simulation without considering martensite volume expansion is done by simple applying tensile load on ferrite–martensite composite structure. 3D RVE simulation with martensite volume expansion is done by two steps, in first step expand the martensite volume according to Eq. (3) and in second step apply tensile load. In this work, martensite volume expansion is considered very similar to thermal expansion. During the martensite volume expansion, martensite and ferrite become stressed solely due to maintained compatibility between two phases, as ferrite volume remains unchanged and martensite volume increases. Due to martensite volume expansion yielding becomes gradual, material shows higher strain hardening as a result stress–strain curve lies above and early necking compared to simulation without martensite volume expansion for DP 590 steel, but as the martensite volume percentage is less than the effect of martensite volume expansion is very small. Details of stress and strain distribution within the actual microstructure due to martensite volume expansion are discussed in latter part of this section.

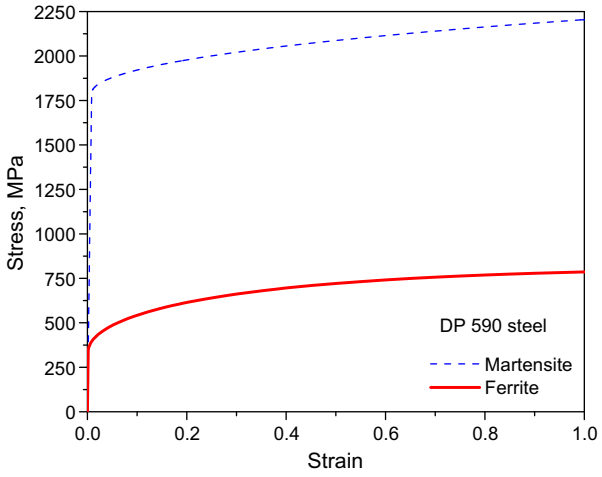

Fig. 3. Flow curve of ferrite and martensite for DP 590 steel.

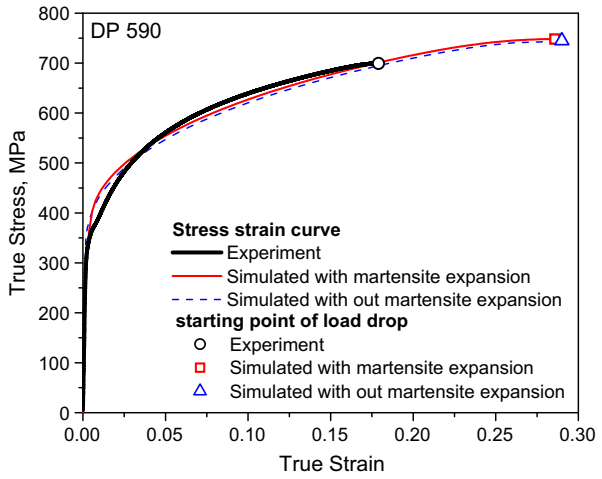

Fig. 4. Comparison of experimental and simulated stress strain curve of DP 590 steel.

Two extreme conditions iso-stress and iso-strain are schematically shown in 2D microstructure in Fig. 5. 3D RVE simulations are done by considering without martensite volume expansion in ABAQUS. Fig. 6 shows that early necking in iso-stress condition and no

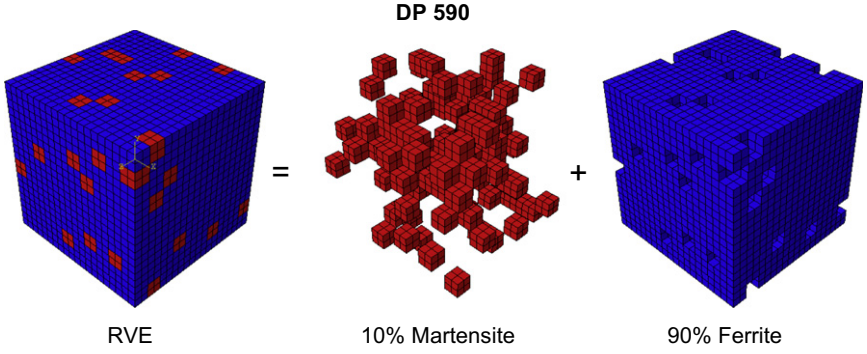

Fig. 2. 3D RVE model used for DP 590 steel with their microstructural constituents.

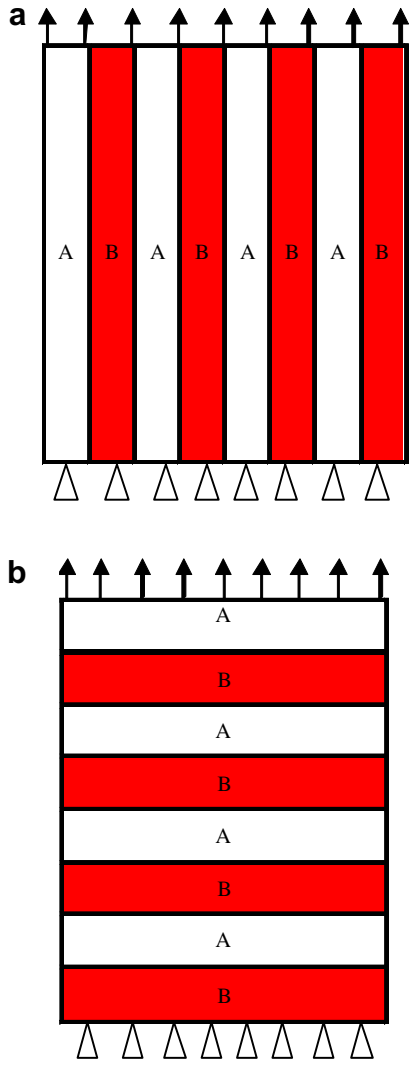

Fig. 5. Schematic diagram of (a) iso-strain and (b) iso-stress condition ('A' and 'B' are two phases).

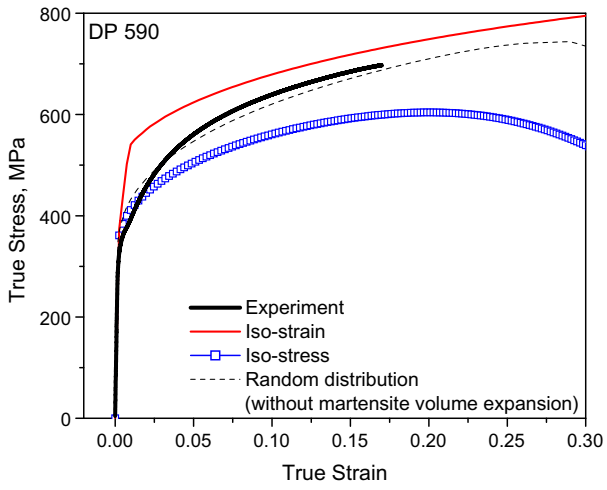

Fig. 6. DP 590 steel: comparison of stress strain curve among experimental and simulated by random distribution, iso-stress, iso-strain conditions.

necking in iso-strain condition, and for random martensite distribution necking occurs at higher strain in comparison to iso-stress

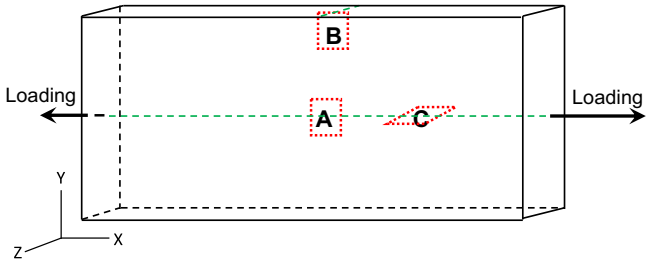

Fig. 7. Microelements in three different locations of a sheet specimen under tensile loading.

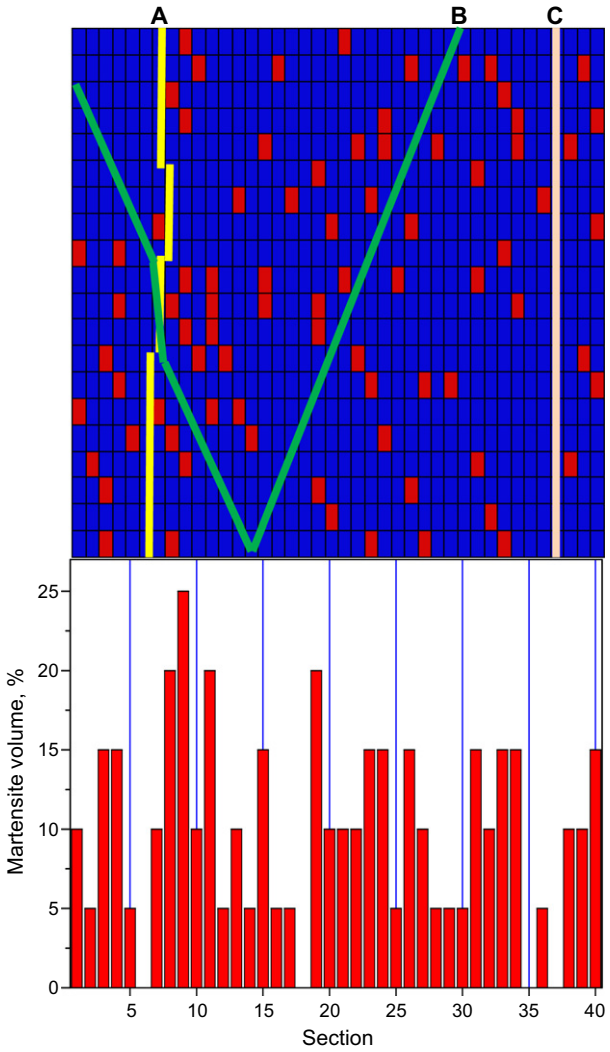

Fig. 8. 2D RVE of DP 590 (10% martensite) showing deformation localization in three different position of a tensile sheet in undeformed shape.

condition. The iso-stress and iso-strain conditions are discussed here to understand the property of banded microstructure with loading direction.

3.3. Microscopic simulation with 2D RVE

In order to examine the effects of different loading conditions on the 2D RVE, three different locations in the tensile specimen are considered. Fig. 7 schematically illustrates the three representative locations on a uniaxial tensile specimen. The region "B"

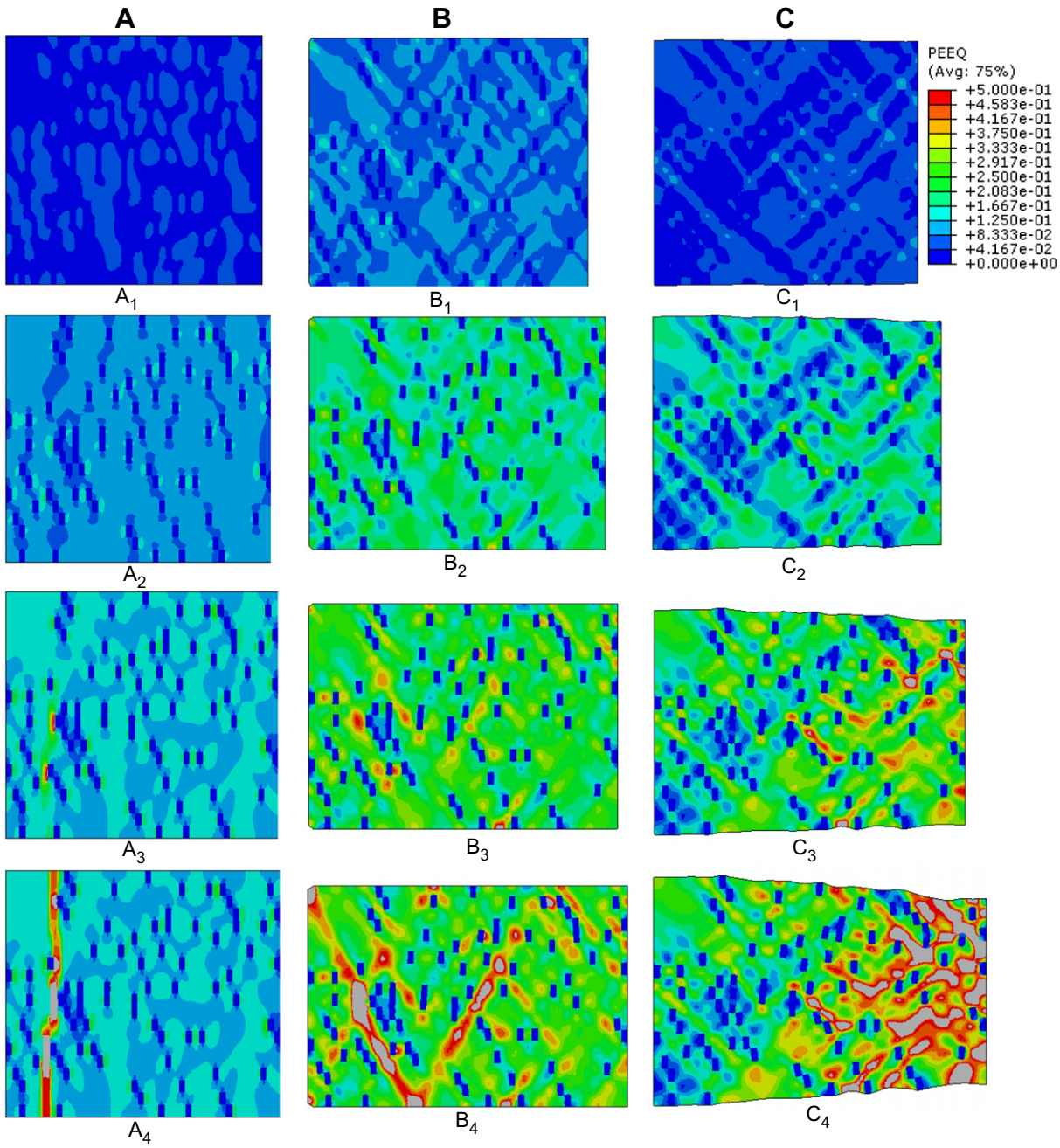

Fig. 9. DP 590 steel: distribution of equivalent plastic strain in three different locations of a sheet specimen under tensile loading, A, B and C (Fig. 7); for A position average strain (%) A_1: 2.5, A_2: 8.0, A_3: 11.1, A_4: 12.1; for B position average strain (%) B_1: 8.0, B_2: 18.0, B_3: 24.0, B_4: 28.5; for C position average strain (%) C_1: 4.0, C_2: 12.0, C_3: 20.0, C_4: 26.0.

shows a local shear failure mode whereas the region "A" shows a local split failure mode during experimentation. This is possibly due to different loading conditions, i.e., load triaxialities, on the material points in those regions [35].

Suppose, 2D RVE (Fig. 7) "A" and "B" are located in the x–y plane and the stresses along the z direction may be considered to be zero as the in-plane dimensions of the sample is much larger than its thickness. For the region "C", located in the x–z plane, the stress state can be considered to be under plane strain because the width of the sheet specimen is much larger than its thickness. Therefore, the materials in the regions "A" and "B" can be considered under the plane stress state and materials in the region "C" can be considered under plane strain state. The lateral constraints on "A" and "B" are different because the lateral sides of the region "B", close to the free boundary of the specimen, can be considered to have no constraint while the lateral sides of the region "A", located near the center of the specimen, are confined not to have any displacement in the y direction. Since the 2D RVE "B" is generated based on the microstructure level, multi-point constraints are applied at the top and bottom surfaces of the 2D RVE such that all the nodes along the top and bottom edges have the same displacements in the y direction. No lateral constraints are applied for region "C" because it is closer to the free boundary of the specimen.

Finite element simulations are conducted in ABAQUS to examine the failure modes of the 2D RVE under the boundary conditions representing the three regions of "A", "B" and "C". Plane stress

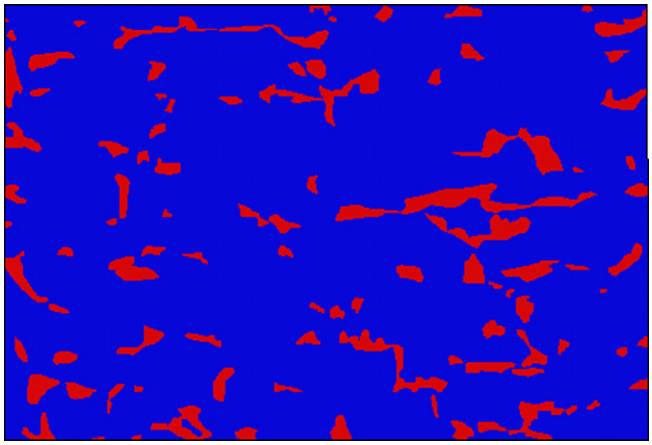

Fig. 10. SEM microstructure used for 2D RVE simulation of DP 590 steel.

elements (CPS3) with and without lateral constraints are used for regions "A" and "B", and plane strain elements (CPE3) with no lateral constraints are used for region "C". In order to simulate the uniaxial tensile loading, all the nodes along the right edge are given the same displacements in the x direction while they can freely move in the y direction during the tensile loading. Here, all the nodes along the left edge are constrained not to move in the x direction, but are allowed to move freely in the y direction.

To study the plastic strain localization from the incompatible deformation between the harder martensite phase and softer ferrite matrix, 2D RVE is generated by random distributed martensite in ferrite matrix which is shown in Fig. 8. Material properties of ferrite and martensite used for this 2D RVE simulation is shown in Fig. 3 for DP 590 steel. Average martensite volume fraction is maintained 10%, and in individual cross section perpendicular to loading direction martensite volume fraction is shown in Fig. 8. Position of deformation localization obtained from simulation in different three regions of "A", "B" and "C" are also shown in Fig. 8. Fracture/failure generally initiated where strain localization takes place; because void initiation, growth and coalition or decohesion between ferrite–martensite take place at higher strained region, and local strain increases drastically in the strain localization zone. Therefore, strain localization zone can be considered as an early stage of fracture/failure zone.

Under plane stress with lateral constraints for region "A", Fig. 9 shows a vertical split failure mode perpendicular to the loading direction with predicted failure strain of 12.1%, much less than that of region "B". This prediction correlates well with the observed failure mode for region "A" by Sun et al. [22,23] and Choi et al. [24].

Under plane stress with no lateral constraints for region "B", Fig. 9 shows a dominant shear failure mode being developed under uniaxial loading. Detailed examination of the deformation process is shown in Fig. 9 indicates that, yielding occurs mainly in the ferrite grains during the early stages of the deformation process. At an overall strain level of 28.5%, the regions with highest equivalent plastic strains begin to localize, which lead to the final shear band failure. These predicted deformation behaviors are in good agreements with the experimentally observed fracture behavior for DP steels [36].

Since perfect bonding between the ferrite and martensite is assumed in this study and no debonding at the grain boundary is modeled, the predicted sites for strain localization can potentially be viewed as the sites for void nucleation in the conventional sense and, therefore, the final shear failure/fracture is predicted as the result of growth and coalescence of these voids.

Under plane strain with no lateral constraints, i.e., region "C", Fig. 9 predicts significant through thickness thinning of the sample. Even though localized hot spots with high equivalent plastic strains do develop at overall strain level of 26%, no distinctive macroscopic coalescence of these regions are predicted under this loading condition, and the final specimen through-thickness failure is predicted in the form of necking.

The failure modes predicted under different loading conditions are similar observation to Sun et al. [22,23] and Choi et al. [24]. These results clearly indicate that the lateral constraints and stress triaxiality dominate the failure mode of the DP steel under examination.

3.4. Microscopic simulation with 2D RVE generated from SEM microstructure

Fig. 10 shows actual SEM microstructures after image processing of DP 590 steel sheet. The SEM picture is taken from the

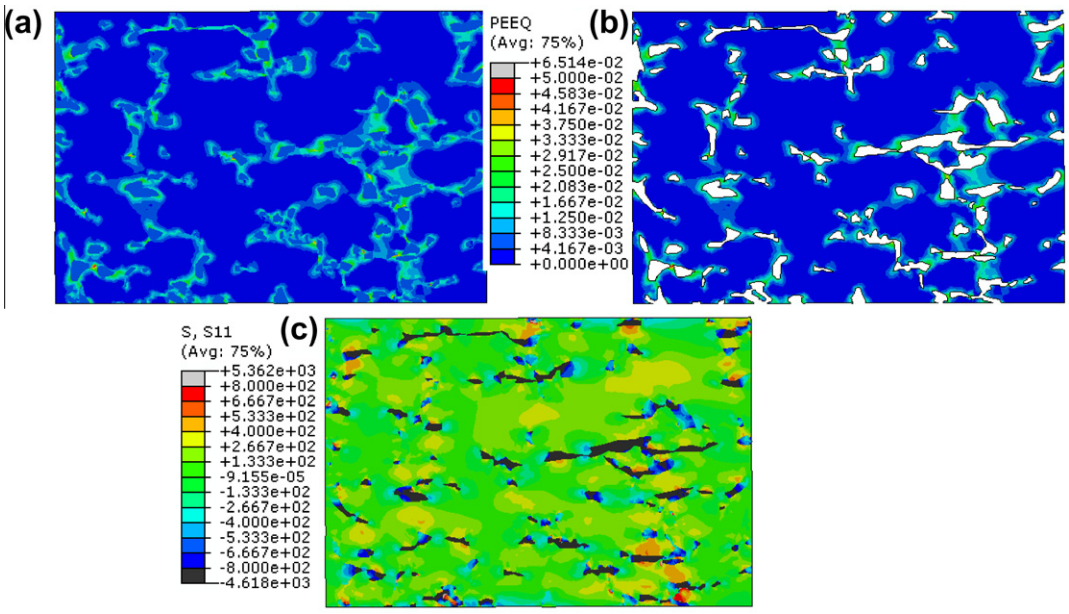

Fig. 11. Distribution of equivalent plastic strain and stress in horizontal direction after volume expansion of martensite: DP 590 steel: (a) equivalent plastic strain, (b) equivalent plastic strain of only ferrite and (c) stress in horizontal direction.

mid-plane along rolling direction of the steel sheet. The microstructure of DP 590 steel is shown in Fig. 10, and it clearly shows the ferrite and martensite phases with two different colors. Meshing is done in HyperMesh and meshed picture is imported in ABAQUS for further analysis. Boundary conditions are exactly same as used in previous 2D RVE simulation. Material properties for ferrite and martensite phases which are shown in Fig. 3 are separately specified in the finite element model. It should be noted that no prescribed failure criterion or imperfection are in the forms of evolving voids and/or damage is used for the ferrite and martensite phases in predicting the overall stress versus strain behaviors of the DP steel. As it will be discussed in detail below, the plastic strain localization is caused by the incompatible plastic deformations accumulated in the two constituent phases during the deformation process, and the ultimate failure of the material is triggered by this initial microstructural inhomogeneity in the form of the coalescence of the highly strained regions in the RVE.

In DP steel ferrite–martensite microstructure is obtained by intercritical annealing in the austenite–ferrite region followed by water quenching. Volume expansion occurs during austenite to martensite transformation, which results elastically and plastically deformed zone in ferrite adjacent to martensite island [16]. This elastically and plastically deformed zone in ferrite i.e. residual stress has an impact on mechanical properties of DP steels. Fig. 11 shows the distribution of equivalent plastic strain and stress in horizontal direction after volume expansion of martensite in DP 590 steel. In the finite element simulation, only volume expansion of martensite is considered according to Eq. (3), cooling effect after

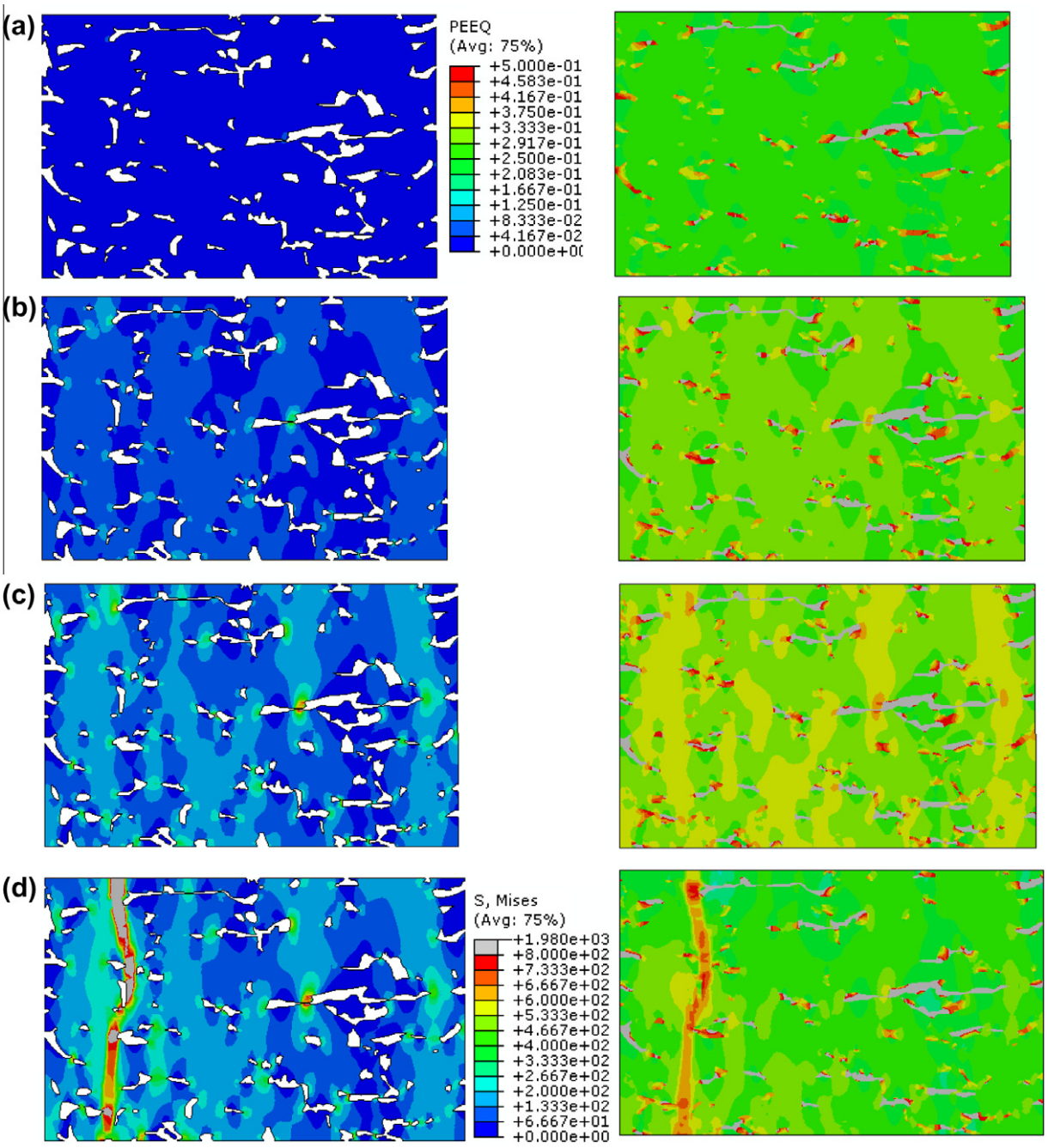

Fig. 12. DP 590: distribution of equivalent plastic strain (only ferrite) and von Mises stress for region "A" at the various average strain levels of (a) 1.25%, (b) 4.0%, (c) 6.5% and (d) 8.3%.

martensite transformation is neglected in the simulation. Fig. 11c shows the stress in horizontal direction after volume expansion of martensite of DP 590 steel. In the Fig. 11c, martensite shows compressive stress and ferrite shows tensile stress. The stress distributions are not uniform through the ferrite and martensite, depending upon the distribution and shape of martensite in ferrite matrix stress field is also varied.

Distributions of the equivalent plastic strain and von Mises stress are illustrated in Fig. 12 for DP 590 steel at various deformation stages for region "A". With lateral constraints, multiple vertical bands with high equivalent plastic strain are predicted within the 2D RVE of DP 590 perpendicular to the loading direction. Initial strain localization occurs at the top corner left side and almost middle position of the 2D RVE of DP 590 at average strain level of 6.5%. The strain localization progresses from left side top corner and localize throughout the cross section in an almost vertical band in left side of 2D RVE of DP 590 in average strain of 8.3%. Whereas, strain localization from middle position of the 2D RVE of DP 590 is unable to propagate on the bottom half, before that of the cross section strain localization from left corner due to martensite island distribution.

Fig. 13 depicts the equivalent plastic strain and von Mises stress evolution of DP 590 steel at various deformation stages for region "B" on deformed configurations. Multiple bands with high equivalent plastic strain are predicted within the 2D RVE along the maximum shear direction. Under plane stress state with lateral constraints, strain localization predicted perpendicular to the loading direction. Initial strain localization arises at the top left side corner of the 2D RVE of region "A" at average strain level of 6.5%. Whereas, initial strain localization starts at much higher strain level of 17.5% from top left corner and middle of 2D RVE of DP 590 for region "B", and the strain localization starts in a band along the maximum shear direction. Growth of strain localization band observed along the maximum shear direction from both top left corner and middle of 2D RVE of DP 590 for region "B", but from top left corner first strain localization band propagates throughout the cross section. The final failure occurs at average strain of 23.7%. Therefore, strain localization band is perpendicular to loading

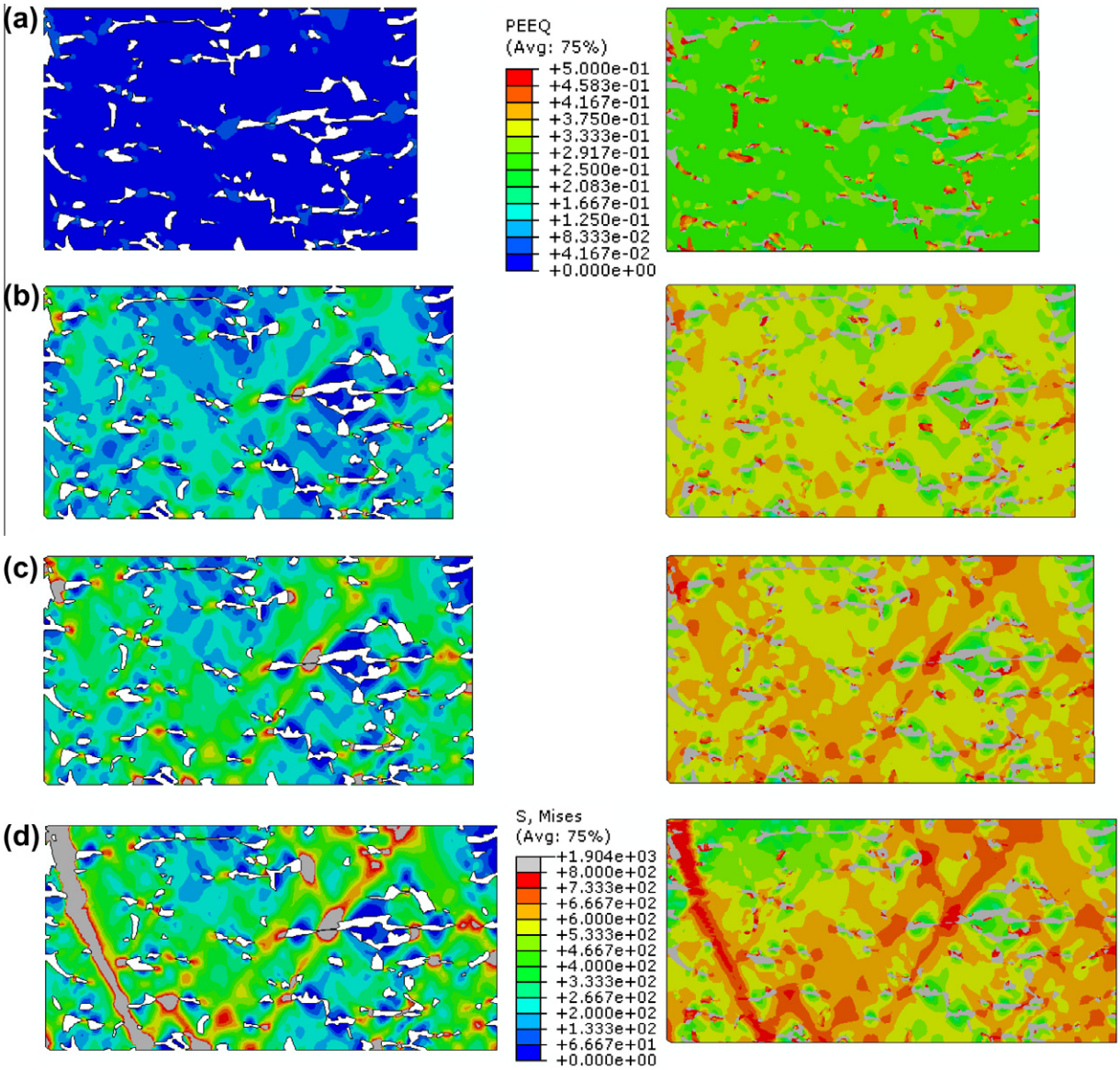

Fig. 13. DP 590: distribution of equivalent plastic strain (only ferrite) and von Mises stress for region "B" at the various average strain levels of (a) 2.5%, (b) 12.5%, (c) 17.5% and (d) 23.7%.

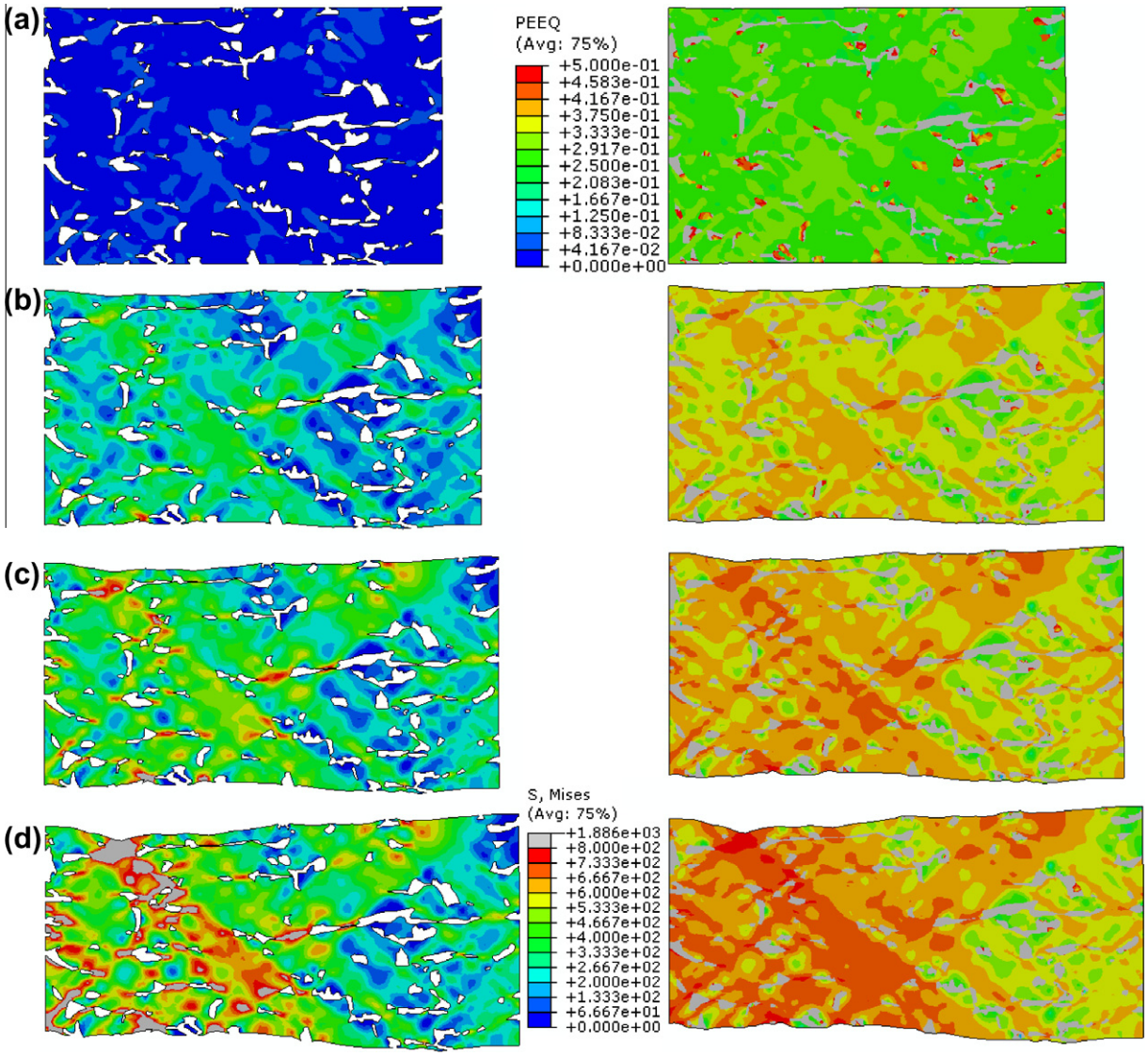

Fig. 14. DP 590: distribution of equivalent plastic strain (only ferrite) and von Mises stress for region "C" at the various average strain levels of (a) 2.5%, (b) 12.5%, (c) 17.5% and (d) 22.5%.

direction i.e. along the maximum principal stress direction for region "A", whereas strain localization band is at an angle to loading direction i.e. along the maximum shear stress direction for region "B".

For the region "C", distributions of the equivalent plastic strain and von Mises stress of DP 590 steel at various deformation stages are shown in Fig. 14. Even though some degree of shear localization is predicted for the initial loading stage, the final specimen failure under this loading condition is again predicted as severe necking similar to that of random distributed martensite microstructure of DP 590 which is already shown in Fig. 9.

4. Conclusions

The ductile failure of dual phase steels is predicted in this study in the form of plastic strain localization resulting from the incompatible deformation between the harder martensite phase and the softer ferrite matrix. Using the microstructure inhomogeneity is the only source of imperfection, failure is predicted as the natural outcome of plastic instability is in the form of localized plastic strain in RVE during the deformation process. Actual SEM microstructure of DP 590 steel and simulated microstructure by random distributed martensite in ferrite matrix is used as 2D RVEs in two dimensional finite element calculations. It is found that the local failure mode is closely related to the stress state in the material. Under plane stress state with free lateral boundary, shear dominant failure mode develops and leads to final failure of the 2D RVE. If the lateral boundary is strictly constrained, the failure mode changes to split mode perpendicular to the loading direction. Whereas, under plane strain state with no lateral boundary constraint local failure happens due to severe necking. Each predicted failure mode is in good agreement with the local failure mode observed in the uniaxial tensile tests of the DP steel sheet specimen reported by Sun et al. [23]. This determination of strain localization is very much helpful to understand failure/fracture modes in this dual phase steel, because strain localization can be considered as the early stage of failure/fracture.

Acknowledgements

Author likes to acknowledge Mr. Abhay Kumar, Dr. Saurabh Kundu and Dr. Monideepa Mukherjee, R&D, Tata Steel Limited,

Jamshedpur, India and Dr. Soumitra Tarafder, National Metallurgical Laboratory, Jamshedpur, India for their valuable suggestions.

References

[1] Davies RG. The deformation behavior of a vanadium-strengthened dual phase steel. Metall Trans 1978;9A:41–52.
[2] Thomas G, Koo JY. In: Kot RA, Morris JW, editors. Structure and properties of dual-phase steels. Warrendale, PA: TMS-AIME; 1979. p. p. 183.
[3] Erdogan M, Tekeli S. The effect of martensite particle size on tensile fracture of surface-carburised AISI 8620 steel with dual phase core microstructure. Mater Des 2002;23(7):597–604.
[4] Bag A, Ray KK, Dwarakadasa ES. Influence of martensite content and morphology on tensile and impact properties of high-martensite dual-phase steels. Metall Trans 1999;30A:1193.
[5] Lanzillotto CAN, Pickering FB. Structure property relationships in dual phase steel. Met Sci 1982;16(N8):371–82.
[6] Ghadbeigi H, Pinna C, Celotto S, Yates JR. Local plastic strain evolution in a high strength dual-phase steel. Mater Sci Eng, A 2010;527(18–19):5026–32.
[7] Al-Abbasi FM, Nemes JA. Micromechanical modeling of dual phase steel. Int J Mech Sci 2003;45(9):1449–65.
[8] Mazinani M, Poole WJ. Effect of martensite plasticity on the deformation behavior of a low-carbon dual-phase steel. Metall Trans 2007;38A:328.
[9] Pickering FB. Advances in the physical metallurgy and applications of steels. Springer; 1981. p. 5–25.
[10] Tomita Y. Effect of morphology of second-phase martensite on tensile properties of Fe-0.1C dual phase steels. J Mater Sci 1990;25:5179–84.
[11] Byun TS, Kim IS. Tensile properties and inhomogeneous deformation of ferrite–martensite dual-phase steels. J Mater Sci 1993;28:2923–32.
[12] Shen HP, Lei TC, Liu JZ. Microscopic deformation behavior of martensitic–ferritic dual-phase steels. Mater Sci Technol 1986;2:28–33.
[13] Rashid MS, Cprek ER. Relationship between microstructure and formability in two high-strength low-alloy steels. In: Niemeier BA, Schmieder AK, Newby JR, editors. Formability topics-metallic materials, ASTM STP 647. Philadelphia, PA: American Society for Testing and Materials; 1978. p. 174–90.
[14] Leslie WC. The physical metallurgy of steels. New York, NY: McGraw-Hill; 1981. p. 216–223.
[15] Bourell DL, Rizk A. Influence of martensite transformation strain on the ductility of dual-phase steels. Acta Metall 1983;31:609–17.
[16] Liedl U, Traint S, Werner EA. An unexpected feature of the stress–strain diagram of dual-phase steel. Comp Mater Sci 2002;25:122–8.
[17] Safikhani AR, Hashemi R, Assempour A. Some numerical aspects of necking solution in prediction of sheet metal forming limits by strain gradient plasticity. Mater Des 2009;30(3):727–40.
[18] Oh CK, Kim YJ, Baek JH, Kim YP, Kim W. A phenomenological model of ductile fracture for API X65 steel. Int J Mech Sci 2007;49(12):1399–412.
[19] Siad L, Ouali MO, Benabbes A. Comparison of explicit and implicit finite element simulations of void growth and coalescence in porous ductile materials. Mater Des 2008;29(2):319–29.
[20] Zhang ZL, Thaulow C, Ødegård J. A complete Gurson model approach for ductile fracture. Eng Fract Mech 2000;67(2):155–68.
[21] Chatzigeorgiou G, Charalambakis N. Instability analysis of non-homogeneous materials under biaxial loading. Int J Plast 2005;21:1970–99.
[22] Sun X, Choi KS, Soulami A, Liu WN, Khaleel MA. On key factors influencing ductile fractures of dual phase (DP) steels. Mater Sci Eng, A 2009;526:140–9.
[23] Sun X, Choi KS, Liu WN, Khaleel MA. Predicting failure modes and ductility of dual phase steels using plastic strain localization. Int J Plast 2009;25:1888–909.
[24] Choi KS, Liu WN, Sun X, Khaleel MA. Microstructure-based constitutive modeling of TRIP steel: prediction of ductility and failure modes under different loading conditions. Acta Mater 2009;57:2592–604.
[25] Choi KS, Soulami A, Liu WN, Sun X, Khaleel MA. Applicability of micromechanics model based on actual microstructure for failure prediction of DP steels. SAE Int J Mater Manuf 2009;2(1):241–9.
[26] Paul SK. Micromechanics based modeling of dual phase steels: prediction of ductility and failure modes. Comput Mater Sci 2012;56:34–42.
[27] Paul SK. Micromechanics based modeling to predict flow behavior and plastic strain localization of dual phase steels. Comput Mater Sci 2012;63:66–74.
[28] Ohata M, Suzuki M, Ui A, Minami F. 3D-Simulation of ductile failure in two-phase structural steel with heterogeneous microstructure. Eng Fract Mech 2010;77(2):277–84.
[29] ASTM Standard E8, 2003. Standard test methods for tension testing of metallic materials ASTM International. West Conshohocken, PA; 2003.
[30] Sodjit S, Uthaisangsuk V. Microstructure based prediction of strain hardening behavior of dual phase steel. Mater Des 2012;41:370–9.
[31] Uthaisangsuk V, Prahl U, Bleck W. Modelling of damage and failure in multiphase high strength DP and TRIP steels. Eng Fract Mech 2011;78:469–86.
[32] Pickering FB. The effect of composition and microstructure on ductility and toughness. In: towards improved ductility and toughness, Tokyo: Climax Molybdenum Company; 1971. p. 9–32.
[33] Park SH. Microstructural evolution of hot rolled TRIP steels during cooling control. In: 40th mechanical working and steel processing conference. ISS/AIME, Pittsburgh; October 1998. p. 283–291.
[34] ABAQUS analysis user's manual. Version 6.8; 2008.
[35] Bai Y, Wierzbicki T. A new model of metal plasticity and fracture with pressure and lode dependence. Int J Plast 2007;24:1071–96.
[36] Erdogan M. The effect of new ferrite content on the tensile fracture behavior of dual phase steels. J Mater Sci 2002;37:3623–30.